arXiv:1309.2131v2 [physics.bio-ph] 14 Jan 2015

# Towards atomistic resolution structure of phosphatidylcholine glycerol backbone and choline headgroup at different ambient conditions

Alexandru Botan,[*] Andrea Catte,[†] Fernando Favela, Patrick Fuchs,[‡] Matti Javanainen,[§] Waldemar Kulig,[§] Antti Lamberg,[¶] Markus S. Miettinen,[‖] Luca Monticelli,[**] Jukka Määttä,[††] Vasily S. Oganesyan,[†] O. H. Samuli Ollila,[‡‡] Marius Retegan,[§§] Hubert Santuz,[¶¶] and Joona Tynkkynen[§]

Phospholipids are essential building blocks of biological membranes. Despite of vast amount of accurate experimental data the atomistic resolution structures sampled by the glycerol backbone and choline headgroup in phoshatidylcholine bilayers are not known. Atomistic resolution molecular dynamics simulation model would automatically resolve the structures giving an interpretation of experimental results, if the model would reproduce the experimental data. In this work we compare the C-H bond vector order parameters for glycerol backbone and choline headgroup between 14 different atomistic resolution models and experiments in fully hydrated lipid bilayer. The current models are not accurately enough to resolve the structure. However, closer inspection of three best performing models (CHARMM36, GAFFlipid and MacRog) suggest that improvements in the sampled dihedral angle distributions would potentilly lead to the model which would resolve the structure. Despite of the inaccuracy in the fully hydrated structures, the response to the dehydration, i.e. P-N vector tilting more parallel to membrane normal, is qualitatively correct in all models. The CHARMM36 and MacRog models describe the interactions between lipids and cholesterol better than Berger/Höltje model. This work has been, and continues to be, progressed and discussed through the blog: nmrlipids.blogspot.fi. Everyone is invited to join the discussion and make contributions through the blog. The manuscript will be eventually submitted to an appropriate scientific journal. Everyone who has contributed to the work through the blog will be offered coauthorship. For more details see: nmrlipids.blogspot.fi.

[*] The authors are listed in alphaphetical order.; Institut Lumière Matière, UMR5306 Université Lyon 1-CNRS, Université de Lyon 69622 Villeurbanne, France
[†] University of East Anglia, Norwich, United Kingdom
[‡] Institut Jacques Monod, CNRS, Universit Paris Diderot, Sorbonne Paris Cit, Paris, France
[§] Tampere University of Technology, Tampere, Finland
[¶] Department of Chemical Engineering, Kyoto University, Kyoto, Japan
[‖] Fachbereich Physik, Freie Universitt Berlin, Berlin, Germany
[**] 5IBCP, CNRS UMR 5086, Lyon, France
[††] Aalto University, Espoo, Finland
[‡‡] **Author to whom correspondence may be addressed. E-mail: samuli.ollila@aalto.fi.**; Helsinki Biophysics and Biomembrane Group, Department of Biomedical Engineering and Computational Science, Aalto University, Espoo, Finland
[§§] Max Planck Institute for Chemical Energy Conversion, Mlheim an der Ruhr, Germany
[¶¶] INSERM, U1134, DSIMB; Institut National de la Transfusion Sanguine (INTS); Laboratoire d'Excellence GR-Ex, Paris, France; Universit Paris Diderot, Sorbonne Paris Cit, Paris, France

## I. INTRODUCTION

Phospholipids containing different polar headgroups and different acyl chains are essential building blocks of biological membranes. Lamellar phospholipid bilayer structures have been widely studied with various experimental and theoretical techniques as a simple model for the biological membranes [1–8]. Phospholipid molecules are composed of hydrophobic acyl chains and hydrophilic headgroup, which are connected by glycerol backbone, see Fig. 1 for the structure of 1-palmitoyl-2-oleoylphosphatidylcholine (POPC). The behaviour of the acyl chains in a bilayer is relatively well understood [1–5, 8, 9]. The structures sampled by the glycerol backbone and choline in liquid bilayer state, however, are not fully resolved since even the most accurate scattering and Nuclear Magnetic Resonance (NMR) techniques give only a set of values that the structure has to fulfill, but there is no unique way to derive the actual structure from these parameters [9–18]. Some structural details have been extracted from crystal structure, $^1$H NMR studies and Raman spectroscopy [19–25] but general consensus about the structures sampled in the liquid state have not been reached [9–18, 24, 25]. On the other hand, the glycerol backbone structures are similar for various biologically relevant lipid species (phosphatidylcholine (PC), phosphatidylethanolamine (PE) and phosphatidylglycerol (PG)) in various environments [26] and the headgroup choline structures are similar in model membranes and real cells (mouse fibroblast L-M cell) [27]. Thus, the resolvation of phosphatidylcholine glycerol backbone and choline structures would be useful for understanding wide range of different biological membranes.

Classical atomistic resolution molecular dynamics simulations have been widely used to study lipid bilayers [2–7]. As these models provide an atomistic resolution description of the whole lipid molecule, they have potential to resolve the glycerol backbone and headgroup structures. In particular, the experimental C-H bond order parameters for the glycerol backbone ($g_1$, $g_2$ and $g_3$) and choline ($\alpha$ and $\beta$) segments (see Fig. 1 for definitions) are among the main parameters used in attempts to derive the structures from experimental data [10–13, 15, 16, 18]. These parameters are also routinely compared between experiments and simulations for the acyl chains [2–6]. Thus, the structures sampled in a simulation model that reproduces these and other experimental parameters, automatically give an interpretation of the experiments, in other words they can be considered as reasonable atomistic resolution descriptions of the behaviour of lipid molecules in a bilayer.

The glycerol backbone and choline headgroup order parameters have been compared between simulations and experiments in some studies [28–37], however much less frequently than for acyl tail chains [2–6]. The main reason is probably that the existing experimental data for the glycerol backbone and choline headgroups is scattered over many publications and published in a format that is difficult to understand without some NMR expertise. In addition to the order parameters, also dihedral angles for glycerol backbone and headgroup estimated from experiments have been sometimes used to assess the quality of simulation model [28, 38–42].

In this work we first review the most relevant experimental data for the glycerol backbone and choline headgroup order parameters in a phosphatidylcholine lipid bilayer. Then the available atomistic resolution lipid models are carefully compared to the experimental data. The comparison reveals that the CHARMM36 [31], GAFFlipid [33] and MacRog models [37] have the most realistic glycerol backbone and choline structures. We also compare the glycerol backbone and choline structures between the most often used (Berger based) lipid model [43] and the best performing models, to demonstrate that by using the order parameters we can distinguish the more reasonable structures from the less reasonable ones. However, none of the current models is accurate enough to resolve the atomistic resolution stuctures.

In addition to the fully–hydrated single–component lipid bilayers, the glycerol backbone and choline order parameters have been measured under a large number of different conditions. For example, as a function of hydration level [44–46], cholesterol content [35, 47] ion concentration [48–52], temperature [53], charged lipid content [51, 52], charged surfactant content [54], drug molecule concentration [30, 55, 56], and protein content [57, 58] (listing only the publications most relevant for this work and the pioneering studies). Awareness of the existence of this type of data allows the comparison of structural responses to varying conditions between simulations and experiments, which can be used to validate the simulation models and to interpret the original experiments. In this publication we demonstrate the power of this approach for understanding the behaviour of a bilayer as a function of hydration level and cholesterol concentration. Choline headgroup order parameters as function of ion concentration, and their relation to the ion binding affinity, are discussed elsewhere [59].

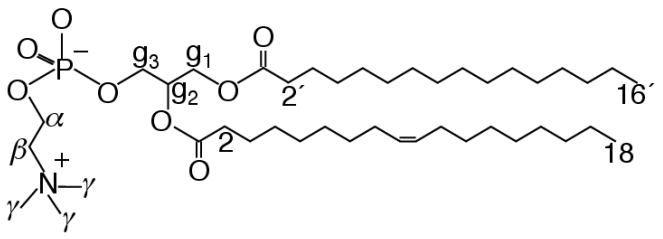



FIG. 1. Chemical structure of 1-palmitoyl-2-oleoylphosphatidylcholine (POPC).

## II. METHODS

### A. Open collaboration

This work has been done as an open collaboration by using nmrlipids.blogspot.fi as an communication platform. The approach is inspired by the Polymath project [60], however there are some essential differences. The manuscript pointing out problems in the glycerol backbone and headgroup structure in the most used molecular dynamics simulation model for lipid bilayers (Berger based models) was used as a starting point [61]. After publishing the initial manuscript, the blog was opened for further contributions and discussion from anyone interested. All the contributions were done publicly through the blog and the blog contributors were offered coauthorship. The final author list is based on the self-assesment of the authors scientific contribution to the project.

Large portion of the used simulation files and scripts are shared through the GitHub organization https://github.com/NMRlipids and Zenodo community https://zenodo.org/collection/user-nmrlipids.

### B. Analysis

The order parameter of a hydrocarbon C-H vector is defined as $S_{\mathrm{CH}} = \frac{3}{2}\langle \cos^2\theta - 1\rangle$, where the average is an ensemble average over the sampled conformations, and $\theta$ is the angle between the C-H bond and the membrane normal. The order parameters can be measured by detecting quadrupolar splitting with $^2$H NMR [62] or by detecting dipolar splitting with $^{13}$C NMR [35, 63–65]. The measurements are based on different physical interactions and also the connection between order parameters and quadrupolar or dipolar splitting are different. The order parameters from the measured quadrupolar splitting $\Delta\nu_Q$ ($^2$H NMR) are calculated using the equation $|S_{\mathrm{CD}}| = \frac{4}{3}\frac{e^2qQ}{h}\Delta\nu_Q$, where the value for the static quadrupole splitting constant is estimated from various experiments to be 170 kHz leading to a numerical relation $|S_{\mathrm{CD}}| = 0.00784 \times \Delta\nu_Q$ [62]. The order parameters from the measured dipolar splitting $d_{\mathrm{CH}}$ ($^{13}$C NMR) are calculated using equation $|S_{\mathrm{CH}}| = \frac{4\pi\langle r_{\mathrm{CH}}^3\rangle}{\hbar\mu_0\gamma_h\gamma_c} d_{\mathrm{CH}}$, where values between 20.2-22.7 kHz are used for $\frac{4\pi\langle r_{\mathrm{CH}}^3\rangle}{\hbar\mu_0\gamma_h\gamma_c}$, depending on the original authors [35, 63–65]. It is important to note that the order parameters measured with different techniques based on different physical interactions are in good agreement with each other (see Results and Discussion), indicating very high quantitative accuracy of the measurements. For more detailed discussion see http://nmrlipids.blogspot.fi/2014/02/accuracy-of-order-parameter-measurements.html

The order parameters from simulations were calculated directly using the definition. For the united atom models the hydrogen locations were generated post-simulationally using the positions of the heavy atoms in the simulation trajectories. The statistical error estimates were calculated for the best performing simulation models by calculating the error of the mean for the average over individual lipids in the system.

It has been recently pointed out that the sampling of individual dihedral angles might be very slow compared to the typical simulation timescales [66]. On the other hand, another recent study shows that the slowest rotational correlation functions of C-H bond ($g_1$) reaches plateau ($S^2_{CH}$) after 200ns in the Berger-POPC-07 [67] model, and that the dynamics of this segment is significantly too slow in simulations compared to the experiments [68]. In practise, less than 200 ns data set is enough for

the order parameter calculation due to the average over different lipid molecules. In conclusion, if the sampling with typical simulation times is not enough for the convergense of the order parameters, then the simulation models has significantly too slow dynamics.

### C. Simulated systems

All simulations are ran with a standard setup for planar lipid bilayer in zero tension and constant temperature with periodic boundary conditions in all directions by using Gromacs software package [69] (version numbers 4.5-4.6) or LAMMPS [70]. The number of molecules, temperatures and the length of simulations for all the simulated systems are listed in Tables I, II and III. Full simulation details are given in the Supplementary Information (SI) or in the original publications if the data is used previously. For some systems also the simulation related files and trajectories are publicly available. The references pointing to simulation details and files are also listed in Tables I, II and III.

TABLE I. Simulated single component lipid bilayers with full hydration. The simulation file data sets marked with * include also part of the trajectory. If simulation data from previously published work has been directly used, the original publication is cited for simulation details. For other systems the simulation details are given in Supplementary Information.

| Force field | lipid | [a]$N_l$ | [b]$N_w$ | [c]T (K) | [d]$t_{sim}$(ns) | [e]$t_{anal}$ (ns) | [f]Files | [g] Details |
|---|---|---|---|---|---|---|---|---|
| Berger-POPC-07 [67] | POPC | 128 | 7290 | 298 | 270 | 240 | [71]* | [68] |
| Berger-DPPC-98 [72] | DPPC | 72 | 2864 | 323 | 140 | 100 | [73] | SI |
| Berger-DMPC-04 [74] | DMPC | 128 | 5097 | 323 | 130 | 100 | [75] | [76] |
| CHARMM36[31] | POPC | 72 | 2242 | 303 | 30 | 20 | [77]* | SI |
| CHARMM36[31] | POPC | 128 | 5120 | 303 | 150 | 100 | - | SI |
| CHARMM36[31] | DPPC | 72 | 2189 | 323 | 30 | 25 | - | SI |
| MacRog[37] | POPC | 288 | 12600 | 310 | 100 | 80 | [78]* | SI |
| GAFFlipid[33] | POPC | 126 | 3948 | 303 | 137 | 32 | [79]* | SI |
| Lipid14[80] | POPC | 72 | 2234 | 303 | 100 | 50 | [81]* | SI |
| Poger[82] | DPPC | 128 | 5841 | 323 | $2\times100$ | $2\times50$ | [83] | SI |
| Slipid[84] | DPPC | 128 | 3840 | 323 | 150 | 100 | [85]* | SI |
| Kukol[86] | POPC | 512 | 20564 | 298 | 50 | 30 | [87]* | SI |
| Chiu et al.[88] | POPC | 128 | 3552 | 298 | 56 | 50 | - | SI |
| Rabinovich et al.[89] | POPC | 128 | 3840 | 303 | 100 | 80 | - | [89] |
| Högberg et al.[29] | DMPC | 98 | 3840 | 303 | 75 | 50 | - | [29] |
| Ulmschneider[90] | POPC | 128 | 3328 | 310 | 100 | 50 | [91]* | SI |
| Tjörnhammar et al.[92] | DPPC | 144 | 7056 | 323 | 200 | 100 | [93]* | [92] |
| CHARMM36-UA [94, 95] | DLPC | 128 | 3840 | 323 | 50 | 20 | [96] | SI |

[a]The number of lipid molecules
[b]The number of water molecules
[c]Simulation temperature
[d]The total simulation time
[e]Time frames used in the analysis
[f]Reference link for the downloadable simulation files
[g]Reference for the full simulation details

## III. RESULTS AND DISCUSSION

### A. Full hydration: Experimental order parameters for glycerol backbone and headgroup

The specific deuteration of $\alpha$-, $\beta$- and $g_3$- segments of dipalmitoylphosphatidylcholine (DPPC) has been successful, allowing the order parameter measurements for these segments by $^2$H–NMR [47–49, 53]. In addition, the order parameters for all glycerol backbone and choline headgroup segments in egg yolk lecithin [63], 1,2-dimyristoyl-sn-glycero-3-phosphocholine (DMPC) [16, 64, 65], 1,2-dioleoyl-sn-glycero-3-phosphocholine (DOPC) [110] and POPC [35, 110] have been measured with

TABLE II. Simulated single component lipid bilayers with varying hydration levels. The simulation file data sets marked with * include also part of the trajectory.

| Force field | lipid | [a] n (w/l) | [b]$N_l$ | [c]$N_w$ | [d]T (K) | [e]$t_{sim}$(ns) | [f]$t_{anal}$ (ns) | [g]Files | [h] Details |
|---|---|---|---|---|---|---|---|---|---|
| Berger-POPC-07 [67] | POPC | 57 | 128 | 7290 | 298 | 270 | 240 | [71]* | SI |
| | POPC | 7 | 128 | 896 | 298 | 60 | 50 | [97]* | SI |
| CHARMM36[31] | POPC | 31 | 72 | 2242 | 303 | 30 | 20 | [77]* | SI |
| | POPC | 15 | 72 | 1080 | 303 | 59 | 40 | [98]* | SI |
| | POPC | 7 | 72 | 504 | 303 | 60 | 20 | [99]* | SI |
| MacRog[37] | POPC | 50 | 288 | 14400 | 310 | 90 | 40 | [100]* | SI |
| | POPC | 25 | 288 | 7200 | 310 | 100 | 50 | [100]* | SI |
| | POPC | 20 | 288 | 5760 | 310 | 100 | 50 | [100]* | SI |
| | POPC | 15 | 288 | 4320 | 310 | 100 | 50 | [100]* | SI |
| | POPC | 10 | 288 | 2880 | 310 | 100 | 50 | [100]* | SI |
| | POPC | 5 | 288 | 1440 | 310 | 100 | 50 | [100]* | SI |
| GAFFlipid[33] | POPC | 31 | 126 | 3948 | 303 | 137 | 32 | [79]* | SI |
| | POPC | 7 | 126 | 896 | 303 | 130 | 40 | [101]* | SI |

[a]Water/lipid molar ratio
[b]The number of lipid molecules
[c]The number of water molecules
[d]Simulation temperature
[e]The total simulation time
[f]Time frames used in the analysis
[g]Reference link for the downloadable simulation files
[h]Reference for the full simulation details

several different implementations of $^{13}$C NMR experiments. The experimental absolute values of glycerol backbone and choline order parameters from various publications are shown in Fig. 2.

In general there is a good agreement between the order parameters measured with different experimental NMR techniques: Almost all the reported values are inside variation of $\pm 0.02$ (which is also the error estimate given by Gross et al. [64]) for all fully hydrated PC bilayer, regardless of the variation in their acyl chain composition and the temperature. Exception are the somewhat lower order parameters sometimes reported having been measured with $^{13}$C–NMR [16, 63, 110]. These experiments have not seen in Fig. 2 as the reported error bars are either relatively large [16, 63], or the spectral resolution is quite low and the numerical lineshape simulations have not been used in the analysis [110]. Therefore it is highly likely that these reported lower order parameters are due to lower experimental accuracy and that we exclude these values from our discussion. Motivated by the high experimental repeatability, we have highlighted in Fig. 2 subjective sweet spots (light blue areas), within which we expect the calculated absolute values of order parameters of a well-performing force field to fall.

In addition to the numerical values, an important feature of the glycerol backbone is the inequality of order parameters for the two hydrogens attached to the same carbon in $g_1$ and $g_3$ segments, while the hydrogens in choline $\alpha$ and $\beta$ segments give equal values. Note that in this work we call the phenomena of inequal order parameters for hydrogens attached to the same carbon as "forking" to avoid confusion with dipolar and quadrupolar splitting in NMR terminology. Forking is also observed experimentally for the $C_2$ carbon in the sn-2 chain of all phosholipids, and it is known to arise from differently sampled orientations of the two C-H bonds, not from two different populations of lipid conformations [111]. The forking in glycerol backbone $g_3$ segment is small ($\approx 0.02$) and some experiments only report the larger or the average value [35, 49]. In contrast, forking is significant for the glycerol backbone $g_1$ segment, whose lower order parameter is close to zero and the larger one has absolute values around 0.13-0.15. Forking was studied in detail by Gally et al. [26], who used E. Coli to stereospecifically deuterate the different hydrogens attached to the $g_1$ or $g_3$ groups in PE lipids, and measured the order parameters from the lipid extract. This experiment gave the lower order parameter when deuterium was in the S position of $g_1$ or R position for $g_3$. Since the glycerol backbone order parameters are very similar irrespective of the headgroup chemistry (PC,PE and PG) or lipid environment [26], it is reasonable to assume that the stereospecifity measured for the PE lipids holds also for the PC lipids.

In Fig. 2 we have shown the absolute values of order parameters as these are accessible with both $^2$H NMR and $^{13}$C NMR techniques. However, $^{13}$C NMR techniques allow also the measurement of the sign of the order parameter [16, 63, 64]. The measured sign is negative for almost all the carbons discussed in this work, only $\alpha$ is positive [16, 63, 64].

Combining the experimental information of the sign [16, 63, 64] and the stereospecifity measurements [26] with the absolute value measurements from various techniques [35, 49, 53, 64, 65] having high quantitative accuracy, the most detailed experimentally available order parameter information for the glycerol backbone and choline segments of POPC is obtained. These

TABLE III. Simulated lipid bilayers with cholesterol. The simulation file data sets marked with * include also part of the trajectory.

| Force field | lipid | [a]$N_l$ | [b]$N_{chol}$ | [c]$N_w$ | [d]T (K) | [e]$t_{sim}$(ns) | [f]$t_{anal}$ (ns) | | |
|---|---|---|---|---|---|---|---|---|---|
| Berger-POPC-07 [67]/Höltje-CHOL-13 [35, 102] | POPC | 128 | 0 | 7290 | 298 | 270 | 240 | [71]* | [68] |
| | POPC | 120 | 8 | 7290 | 298 | 100 | 80 | [103]* | [35] |
| | POPC | 110 | 18 | 8481 | 298 | 100 | 80 | [104]* | [35] |
| | POPC | 84 | 44 | 6794 | 298 | 100 | 80 | [105]* | [35] |
| | POPC | 64 | 64 | 10314 | 298 | 100 | 80 | [106]* | [35] |
| | POPC | 50 | 78 | 5782 | 298 | 100 | 80 | [107]* | [35] |
| CHARMM36[31, 108] | POPC | 128 | 0 | 5120 | 303 | 150 | 100 | - | SI |
| | POPC | 100 | 24 | 4960 | 303 | 200 | 100 | - | SI |
| | POPC | 80 | 80 | 4496 | 303 | 200 | 100 | - | SI |
| MacRog[37] | POPC | 128 | 0 | 6400 | 310 | 400 | 200 | [109]* | SI |
| | POPC | 114 | 14 | 6400 | 310 | 400 | 200 | [109]* | SI |
| | POPC | 72 | 56 | 6400 | 310 | 400 | 200 | [109]* | SI |
| | POPC | 64 | 64 | 6400 | 310 | 400 | 200 | [109]* | SI |
| | POPC | 56 | 72 | 6400 | 310 | 400 | 200 | [109]* | SI |

[a]The number of lipid molecules
[b]number of cholesterol molecules
[c]The number of water molecules
[d]Simulation temperature
[e]The total simulation time
[f]Time frames used in the analysis

data are shown in Fig. 3.

### B. Full hydration: Comparison between simulation models and experiments

The order parameters of the glycerol backbone and headgroup calculated from different force fields for various lipids has been previously compared to experiments [28–37]. The general conclusion from these works seems to be that the CHARMM based [29, 31], GAFFlipid [33] and MacRog [37] force fields perform better for the glycerol backbone and headgroup structures than the Gromos based models [30, 32, 34, 35]. However, none of the studies exploits the full potential of the available experimental data discussed in previous section; the quantitative accuracy, known signs and stereospecific labeling of the experimental order parameters.

To get a general idea about the quality of the glycerol backbone and choline headgroup structures in different models, we calculated the absolute values of the order parameters for these parts from fourteen different lipid models (Table I) and plotted the results together with experimental values in Fig. 2. Two criteria were used to judge the quality of the model: **forkings** there must not be significant forking in the $\alpha$ and $\beta$ carbons, there must be only moderate forking in the $g_3$ carbon and there must be significant forking in the $g_1$ carbon, **absolute values** should be preferably inside to the subjective sweet spots determined from experiments (blue shaded regions in Fig. 2). None of the studied force fields fulfills these criteria, however, three force fields are closer than others: CHARMM36 [31], MacRog [37] and GAFFlipid [33].

The top three models (CHARMM36, MacRog and GAFFlipid) together with the most used lipid model (Berger based model) were subjected to a more careful comparison including the signs and the sterospecific labeling in Fig. 3. The essential additional information given by this comparison is that the sign of the $\beta$ carbon order parameter is correct only in CHARMM36 model.

### C. Full hydration: Atomistic resolution structures in different models

The results in the previous section revealed significant differences of the glycerol backbone and choline headgroup order parameters between different molecular dynamics simulation models. However, it is not straightforward to conclude which kind of structural differences (if any) between the models the results indicate, because the mapping from the order parameters to the structure is not unique. In this section we demonstrate that 1) the differences in order parameters indicate significantly different structural sampling strongly correlating with the dihedral angles of the related bonds, and that 2) the comparison between experimental and simulated order parameters can be used to exclude nonrealistic structural samping in molecular

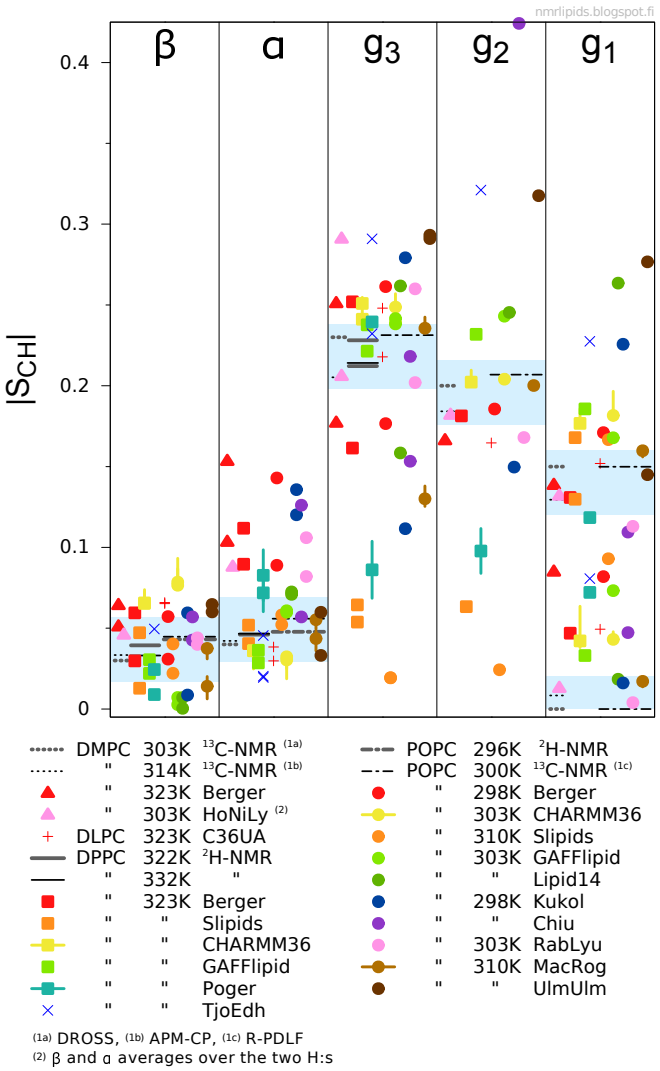



FIG. 2. Order parameteres from simulations listed in Table I and experiments for glycerol and choline groups. The experimental values were taken from the following publications: DMPC 303K from [64], DMPC 314K from [65], DPPC 310K from [53], DPPC 323K from [49], and POPC 298K [35]. The vertical bars shown for some of the computational values are not error bars, but demonstrate that for these systems we had two data sets; the ends of the bars mark the values from the two sets, and the dot marks their measurement-time-weighted average. The Högberg et al. force field in Table I is abbreviated in this figure as HoNiLy, Tjörnhammar et al. as TjoEdh, CHARMM36-UA as C36UA, Rabinovic et al. as RabLyu and Ulmschneider as UlmUlm.

dynamics simulations. The demonstration is done for the dihedral angles defined by the $g_3$-$g_2$-$g_1$-O(sn-1) segments in the glycerol backbone and the N-$\beta$-$\alpha$-O segments in the headgroup. These dihedrals were chosen for demonstration, because significant differences between the models are observed around these segments in Fig. 3. We note that performing a similar comparison through all the dihedrals in all the 14 models would probably give highly useful information to improve the accuracy of simulations, however this is beyond the scope of the current report.

The dihedral angle distributions for the $g_3$-$g_2$-$g_1$-O(sn-1) dihedral calculated from different models are shown in Fig. 4. The distribution is qualitatively different for the Berger-POPC-07 model, showing a maximum in the gaughe$^+$-conformation ($60^o$) compared to all the other models showing a maximum in the trans-conformation ($180^o$). The distributions in all the other models have the same general features, the main difference being that the fraction of configurations in gaughe$^-$-conformation ($-60^o$) is zero for the MacRog, detectable for the CHARMM36 and equally large to the gaughe$^+$ fraction in GAFFlipid. From the results we conclude that most likely the wrongly sampled dihedral angle for the $g_2$-$g_1$ bond explains the significant discrepancy to the experimental order parameters for the $g_1$ segment in the Berger-POPC-07 model (Fig. 3). The result that models preferring the trans conformation for this dihedral gives more realistic order parameters is in agreement with previous crystal structure and $^1$H NMR studies [19–21, 23–25].

The dihedral angle distribution for the N-$\beta$-$\alpha$-O dihedral calculated from the same four models is shown in Fig. 5. Also

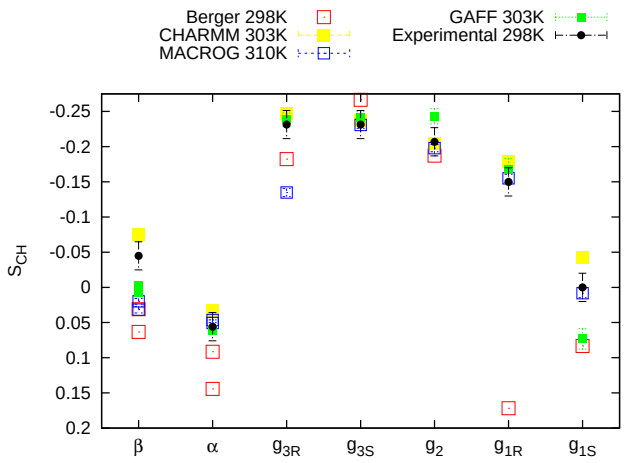



FIG. 3. Order parameteres from simulations with Berger-POPC-07, CHARMM36, GAFFlipid and Macrog force fields together with experimental values for POPC glycerol and choline groups. The magnitudes for experimental order parameters are taken from Ferreira et al. [35], the signs are based on the measurements by Hong et al. [16, 63] and Gross et al. [64], and the R/S labeling is based in the measurements by Gally et al. [26].

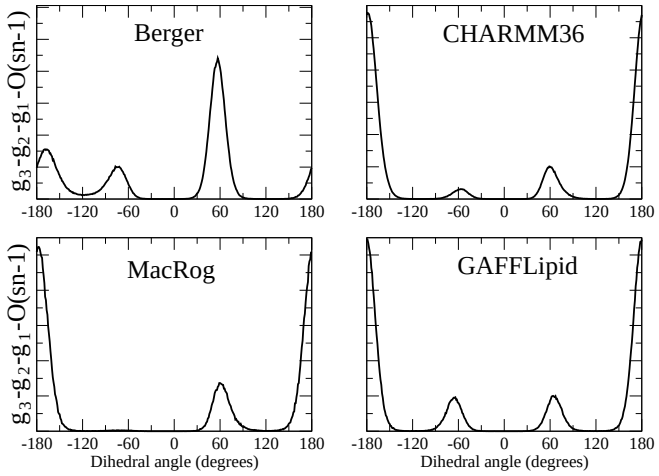



FIG. 4. Dihedral angle distributions for $g_3$-$g_2$-$g_1$-O(sn-1) dihedral from different models (POPC bilayer in full hydration).

for this dihedral there are significant differences in the gauche-trans fractions. The gaughe conformations are dominant in the CHARMM36, in MacRog there are only trans conformations present, and in the Berger-POPC-07 and GAFFlipid gaughe and trans conformation has equal probability. On the other hand comparison of $\alpha$ and $\beta$ order parameters in Fig. 3 reveals that the CHARMM36 is closest to the experimental results being the only model having correct sign (negative) for the $\beta$ order parameter. This result is again in agreement with previous crystal structure, $^1$H NMR and Raman spectroscopy studies [19–22] which suggest that this dihedral has only gaughe conformation in the absense of ions.

The used examples show that the glycerol backbone and headgroup order parameters reflect the atomistic resolution structure and that the comparison with experiments allows the assesment of the quality of the suggested structure. We were able to pinpoint specific problems in the structures in different models and suggest potential improvement strategies. If the improved atomistic resolution molecular dynamics simulation model would reproduce the order parameters and other experimental observables (like chemical shift anisotropy) with experimental accuracy, it would give an interpretation for the atomistic resolution structure of the glycerol backbone and choline [10–13, 15, 16, 18]. The research along these lines is left, however, for future studies.

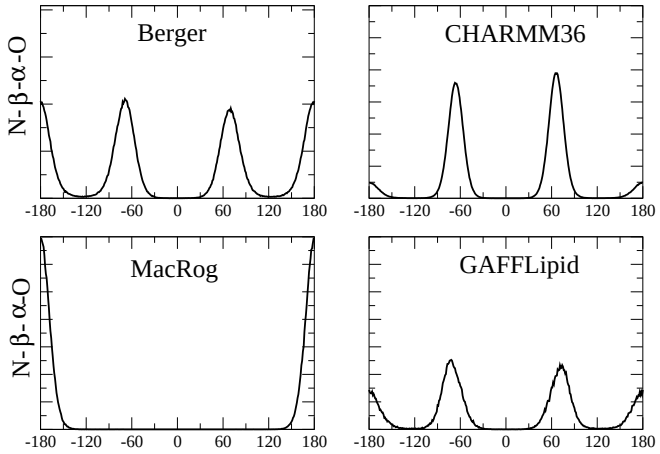



FIG. 5. Dihedral angle distributions for N-$\beta$-$\alpha$-O dihedral from different models (POPC bilayer in full hydration).

### D. Response to dehydration and cholesterol content

In addition to pure phosphatidylcholine bilayers at full hydration, the choline headgroup order parameters have been measured under various different conditions [30, 32, 35, 44–50, 53, 54]. Also the order parameters for the glycerol backbone have been measured with $^{13}$C NMR in dehydrated conditions [46], and as a function of anesthetics [30] and glycolipids [32] for DMPC, and as a function of cholesterol concentration for POPC [35]. Due to the high resolution in the NMR (especially $^{2}$H NMR) experiments, even very small order parameter changes resulting from the varying conditions can be measured (see http://nmrlipids.blogspot.fi/2014/02/accuracy-of-order-parameter-measurements.html for more discussion. However, as already discussed above, it is not simple to deduce the structural changes from order parameter changes [15, 18]. Consequently, comparison of the order parameters between simulations and experiments in different conditions can be used measure the quality of the force field in different situations, and, if the quality is good, to potentially interpret the structural changes in experiments. Here we exemplify such comparison for a lipid bilayer under low hydration levels and mixed with cholesterol. The interaction between ions and phosphatidylcholine bilayer is discussed in a separate work [59].

#### *1. Phospholipid bilayer with low hydration level*

The experimental order parameters available in the literature [44–46] for the glycerol backbone and choline as a function of hydration level are shown in Fig. 6. The independently reported values for choline segments are in good agreement with each other (despite of slight differences in temperature and acyl chain composition), showing increase for both segments with decreasing hydration level. It should be noted that only absolute values were measured in the original experiments [44–46], but we have included the signs measured separately [16, 63, 64]. Consequently, the $\beta$ order parameter with negative sign actually increases with dehydration since the absolute value decreases [44–46]. Slight decrease for the glycerol backbone $g_3$- and $g_2$-order parameters were observed with dehydration, while $g_1$ remained practically unchanged [46].

Lipid bilayer dehydration has been studied also with molecular dynamics simulations [112–117], typically motivated by the discussion about the origin of the "hydration repulsion" [118–120]. However, the used simulation models are not typically compared to the experimental choline and glycerol backbone order parameters (except by Mashl et al. [112]). In Fig. 6 the glycerol backbone and choline order parameters as a function of hydration level are shown for the CHARMM36, MacRog and GAFFlipid models (having the most realistic atomistic resolution structures) together with the Berger based model (which is the most used lipid model). The choline order parameters increase with dehydration in all simulation models, in qualitative agreement with experiments. The measured decrease in both $g_3$ and $g_2$ order parameters with dehydration is reproduced only in CHARMM36.

The qualitative agreement with experiments in all simulation models for the $\alpha$ and $\beta$ order parameters as a function of hydration indicates that the structural response of the choline headgroup to dehydration is somewhat realistic despite the unrealistic structures at full hydration. The most likely explanation is that the choline group orients more parallel to the membrane plane with dehydration due to restricted interlamellar space. Indeed, the P-N angle vector angle with membrane normal as a function of dehydration shows an increase for all models as a function of dehydration in Fig. 7. However, the qualitative agreement in the lipid response to dehydration does not guarantee the correct free energy landscape if the simulation model has incorrect

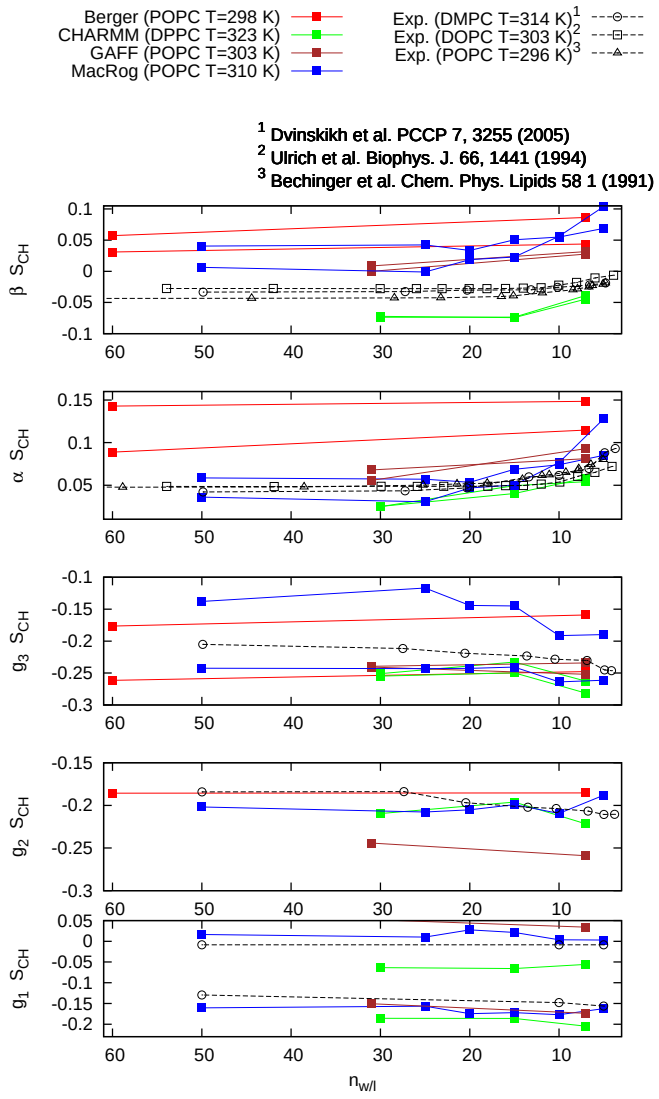



FIG. 6. The effect of dehydration on glycerol and choline order parameters in experiments. The magnitudes of order parameters are measured for DMPC ($^{13}$C NMR) at 314 K [46], for POPC ($^{2}$H NMR) at 296 K [44] and for DOPC ($^{2}$H NMR) at 303 K [45]. The signs are based on the measurements by Hong et al. [16, 63] and Gross et al. [64].

structure. The influence of this issue to dehydration energetics studied with simulations [115, 117] is left for future studies.

The response of the glycerol backbone to dehydration seems to be more subtle than of the choline headgroup as CHARMM36 is the only model that reproduces the decrease in $g_2$ and $g_3$ segments.

### 2. *Phospholipid bilayer mixed with cholesterol*

Phospholipid–cholesterol interactions have been widely studied with theoretical [121–124] and experimental methods [8, 35, 47, 125], since cholesterol is abundant in biological membranes and it has been suggested to be an important player, for example, in domain formation [126, 127]. It is widely agreed that cholesterol orders lipid acyl tails thus decreasing the area per molecule (condensing effect), however, the influence of cholesterol on the lipid headgroup and glycerol backbone are sill debated [121, 126, 127]. For example, it has been suggested that the surrounding lipids shield cholesterol from interactions with water by reorienting their headgroups (“umbrella model”) [121] or that cholesterol acts as a spacer for the headgroups thus increasing their entropy and dynamics (“superlattice model”) [127]. Both of these suggestions have been supported by molecular dynamics simulations [122, 124], and other simulations suggest specific interactions between the glycerol backbone and cholesterol [123], however the glycerol backbone and choline headgroup behaviour as a function of cholesterol content is

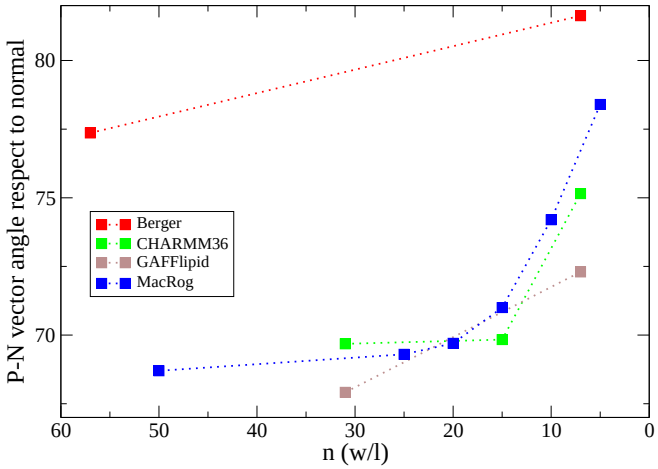



FIG. 7. The angle between membrane normal and P-N vector in choline segment as function of hydration level calculated from different simulations.

not compared to experiments in these studies.

The choline headgroup and glycerol backbone order parameters for POPC measured by $^{13}$C NMR [35] and DPPC choline order parameters measured by $^{2}$H NMR [47] are shown in Fig. 8 as a function of cholesterol content. The agreement between different experimental results is again very good, showing only very modest changes in the choline order parameters as a function of cholesterol content. It should be noted, however, that very small changes are measurable with high resolution $^{2}$H NMR experiments and cholesterol causes a measurable increase in the $\beta$ order parameter and a forking in the $\alpha$ order parameter [47], but these effects are so small that they are barely visible in the scale used in Fig. 8. Further, the effects of cholesterol on the glycerol backbone order parameters for POPC from $^{13}$C NMR experiment [35] is in good agreement with the results for the phosphatidylethanolamine (PE) measured by $^{2}$H NMR [128]. These results further support the idea that the glycerol backbone structural behaviour is independent of the headgroup composition [26] and that the headgroup stucture is independent of the acyl chain region content unless charges are present [27].

In addition to the experimental data, the previously published simulation results from the Berger-POPC-07/Höltje-CHOL-13 model [35], and our results from CHARMM36 and MacRog force fields are shown in Fig. 8. As already pointed out previosly, the Berger-POPC-07/Höltje-CHOL-13 model seriously overestimates the effect of cholesterol on the phospholipid glycerol backbone and choline segments [35]. In contrast, the responses of both CHARMM36 and MacRog are in better agreement with experiments, however CHARMM36 seems to better reproduce the experimentally observed modest changes in the glycerol backbone segments $g_2$ and $g_3$ with high concetrations of cholesterol. Thus we have calculated the glycerol backbone dihedral angle distributions as a function of cholesterol in CHARMM36 (shown in Supplementary material) to resolve the cholesterol induced structural changes. The only detectable change due to the addition of cholesterol is the small decrease of gaughe- and increase of gaughe+ probability of g3-g2-g1-O(sn-1) dihedral.

It should be noted that the CHARMM36 force field parameters (dihedral potentials) for the glycerol backbone have been tuned the dihedral potentials to reproduce the correct order parameters at fully hydrated conditions [31]. This procedure contains a risk of overfitting, which would manifest itself as wrong responses to changing conditions. According to our results, tuning seems not to lead to overfitting problems in the case of dehydration or lipid-cholesterol mixtures.

## IV. CONCLUSIONS

The atomistic resolution structures sampled by the glycerol backbone and choline headgroup in phoshatidylcholine bilayers are not known despite of vast amount of accurate experimental data. Atomistic resolution molecular dynamics simulation model which would reproduce the experimental data would automatically resolve the structures giving an interpretation of experimental results. In this work we have collected and reviewed the experimental C-H bond vector order parameters available in literature. These experimental parameters are then compared to different atomistic resolution simulation models for fully hydrated bilayer, dehydrated bilayer and lipid bilayer containing cholesterol. Our results have led to the following conclusions:

- The C-H bond order parameters measured with different NMR techniques are in good agreement with each others. By combining the experimental results from various sources we concluded that the order parameters for each C-H bond are known with quantitative accuracy of $\pm 0.02$.

- None of the tested models (14 different models) produces the order parameters with the experimental accuracy for fully

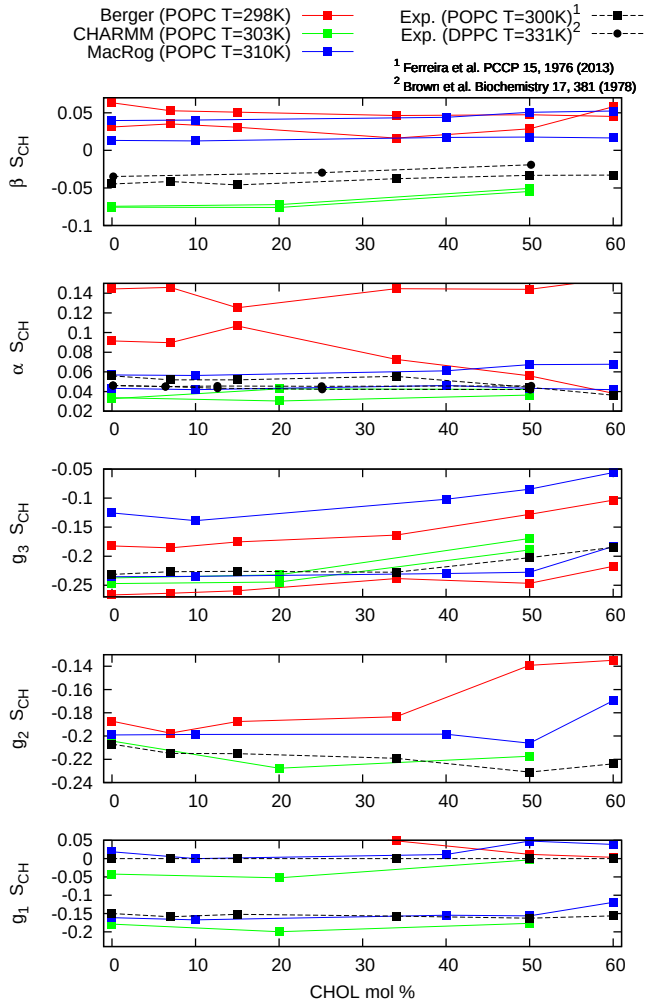



FIG. 8. The effect of cholesterol content on the glycerol backbone and choline order parameters in experiments [35, 47] and simulations with the Berger-POPC-07/Höltje-CHOL-13, CHARMM36 and MacRog force fields. The signs in the experimental values are based on the measurements by Hong et al. [16, 63] and Gross et al. [64]. The most order parameters from Berger-POPC-07/Höltje-CHOL-13 model for $g_1$ are beoynd the y-axis scale.

hydrated phoshatidylcholine lipid bilayer. However, the CHARMM36, GAFFlipid and MacRog models are relatively close. The structures of these models together with the most used lipid model (Berger based) were subjected to more careful studies. The results revealed that the current models are not accurate enough to resolve the atomistic resolution structures sampled by glycerol backbone and choline headgroup. However, the correlation between dihedral angle distributions and order parameter differences was found, suggesting that careful adjustment of dihedral potentials would potentially lead to the model with correct structure.

- Independent of the accuracy for fully hydrated lipid bilayer, all the models reproduced the choline response to the dehydration. This can be explained by the change in the P-N vector tilting more parallel to the membrane which leads to the increase of order parameters despite of the initial configuration. It should be however noted that the correct qualitative response do not necessarily indicate correct energetics.

- The response of glycerol backbone and choline headgroup to the cholesterol content is described more realistically in CHARMM36 and MacRog models than in the Berger based model.

In general, we conclude that the atomistic resolution classical molecular dynamics simulations is extremely convenient tool to give structural interpretation for the high resolution NMR data [129]. However, in the case of phoshatidylcholine glycerol backbone and choline headgroup there is some further model development required.

This work has been, and continues to be, progressed and discussed through the blog: nmrlipids.blogspot.fi. Everyone is invited to join the discussion and make contributions through the blog. The manuscript will be eventually submitted to an appropriate scientific journal. Everyone who has contributed to the work through the blog will be offered coauthorship. For more details

see: nmrlipids.blogspot.fi.

**Acknowledgements:** OHSO acknowledges Tiago Ferreira and Paavo Kinnunen for useful discussions, the Emil Aaltonen foundation for financial support, Aalto Science-IT project and CSC-IT Center for Science for computational resources.

---

[1] R. Lipowsky and E. Sackmann, eds., *Structure and Dynamics of Membranes* (Elsevier, 1995).
[2] D. P. Tieleman, S. J. Marrink, and H. J. C. Berendsen, Biochim. Biophys. Acta **1331**, 235 (1997).
[3] J. B. Klauda, R. M. Venable, A. D. M. Jr., and R. W. Pastor, in *Computational Modeling of Membrane Bilayers*, edited by S. E. Feller (Academic Press, 2008)*Current Topics in Membranes of vol. 60*, pp. 1 – 48.
[4] O. Edholm, in *Computational Modeling of Membrane Bilayers*, edited by S. E. Feller (Academic Press, 2008)*Current Topics in Membranes of vol. 60*, pp. 91 – 110.
[5] D. P. Tieleman, in *Molecular Simulations and Biomembranes: From Biophysics to Function*, edited by M. Sansom and P. Biggin (The Royal Society of Chemistry, 2010), pp. 1–25.
[6] T. J. Piggot, . Pieiro, and S. Khalid, Journal of Chemical Theory and Computation **8**(11), 4593 (2012).
[7] A. Rabinovich and A. Lyubartsev, Polymer Science Series C **55**(1), 162 (2013).
[8] D. Marsh, *Handbook of Lipid Bilayers, Second Edition* (RSC press, 2013).
[9] J. N. Israelachvili, S. Marcelja, and R. G. Horn, Q. Rev. Biophys. **13**, 121 (1980).
[10] J. Seelig, H.-U. Gally, and R. Wohlgemuth, Biochimica et Biophysica Acta (BBA) - Biomembranes **467**(2), 109 (1977).
[11] R. Skarjune and E. Oldfield, Biochemistry **18**(26), 5903 (1979).
[12] R. E. Jacobs and E. Oldfield, Progress in Nuclear Magnetic Resonance Spectroscopy **14**(3), 113 (1980).
[13] J. H. Davis, Biochimica et Biophysica Acta (BBA) - Reviews on Biomembranes **737**(1), 117 (1983).
[14] L. Strenk, P. Westerman, and J. Doane, Biophysical Journal **48**(5), 765 (1985).
[15] H. Akutsu and T. Nagamori, Biochemistry **30**, 4510 (1991).
[16] M. Hong, K. Schmidt-Rohr, and D. Nanz, Biophysical Journal **69**(5), 1939 (1995).
[17] M. Hong, K. Schmidt-Rohr, and H. Zimmermann, Biochemistry **35**(25), 8335 (1996).
[18] D. J. Semchyschyn and P. M. Macdonald, Magnetic Resonance in Chemistry **42**(2), 89 (2004).
[19] H. Hauser, W. Guyer, I. Pascher, P. Skrabal, and S. Sundell, Biochemistry **19**(2), 366 (1980).
[20] H. Hauser, W. Guyer, and F. Paltauf, Chemistry and Physics of Lipids **29**(2), 103 (1981).
[21] H. Hauser, I. Pascher, R. Pearson, and S. Sundell, Biochimica et Biophysica Acta (BBA) - Reviews on Biomembranes **650**(1), 21 (1981).
[22] H. Akutsu, Biochemistry **20**(26), 7359 (1981).
[23] I. Pascher, M. Lundmark, P.-G. Nyholm, and S. Sundell, Biochimica et Biophysica Acta (BBA) - Reviews on Biomembranes **1113**(34), 339 (1992).
[24] H. Hauser, I. Pascher, and S. Sundell, Biochemistry **27**(26), 9166 (1988).
[25] D. Marsh and T. Pli, Chemistry and Physics of Lipids **141**(12), 48 (2006).
[26] H. U. Gally, G. Pluschke, P. Overath, and J. Seelig, Biochemistry **20**(7), 1826 (1981).
[27] P. Scherer and J. Seelig, The EMBO journal **6**(10) (1987).
[28] W. Shinoda, N. Namiki, and S. Okazaki, The Journal of Chemical Physics **106**(13) (1997).
[29] C.-J. Högberg, A. M. Nikitin, and A. P. Lyubartsev, Journal of Computational Chemistry **29**(14), 2359 (2008).
[30] V. Castro, B. Stevensson, S. V. Dvinskikh, C.-J. Högberg, A. P. Lyubartsev, H. Zimmermann, D. Sandstrm, and A. Maliniak, Biochim. Biophys. Acta - Biomembranes **1778**, 2604 (2008).
[31] J. B. Klauda, R. M. Venable, J. A. Freites, J. W. O'Connor, D. J. Tobias, C. Mondragon-Ramirez, I. Vorobyov, A. D. M. Jr, and R. W. Pastor, J. Phys. Chem. B **114**, 7830 (2010).
[32] J. Kapla, B. Stevensson, M. Dahlberg, and A. Maliniak, J. Phys. Chem. B **116**, 244 (2012).
[33] C. J. Dickson, L. Rosso, R. M. Betz, R. C. Walker, and I. R. Gould, Soft Matter **8**, 9617 (2012).
[34] D. Poger and A. E. Mark, Journal of Chemical Theory and Computation **8**(11), 4807 (2012).
[35] T. M. Ferreira, F. Coreta-Gomes, O. H. S. Ollila, M. J. Moreno, W. L. C. Vaz, and D. Topgaard, Phys. Chem. Chem. Phys. **15**, 1976 (2013).
[36] J. Chowdhary, E. Harder, P. E. M. Lopes, L. Huang, A. D. MacKerell, and B. Roux, The Journal of Physical Chemistry B **117**(31), 9142 (2013).
[37] A. Maciejewski, M. Pasenkiewicz-Gierula, O. Cramariuc, I. Vattulainen, and T. Rog, The Journal of Physical Chemistry B **118**(17), 4571 (2014).
[38] A. Robinson, W. Richards, P. Thomas, and M. Hann, Biophysical Journal **67**(6), 2345 (1994).
[39] J. W. Essex, M. M. Hann, and W. G. Richards, Philosophical Transactions of the Royal Society of London B: Biological Sciences **344**(1309), 239 (1994).
[40] V. Kothekar, Ind. J. Biochem. Biophys. **33**, 431 (1996).
[41] M. T. Hyvönen, T. T. Rantala, and M. Ala-Korpela, Biophys. J. **73**, 2907 (1997).
[42] T. H. Duong, E. L. Mehler, and H. Weinstein, Journal of Computational Physics **151**(1), 358 (1999).
[43] O. Berger, O. Edholm, and F. Jähnig, Biophys. J. **72**, 2002 (1997).
[44] B. Bechinger and J. Seelig, Chem. Phys. Lipids **58**, 1 (1991).
[45] A. Ulrich and A. Watts, Biophys. J. **66**, 1441 (1994).

[46] S. V. Dvinskikh, V. Castro, and D. Sandstrom, Phys. Chem. Chem. Phys. **7**, 3255 (2005).
[47] M. F. Brown and J. Seelig, Biochemistry **17**, 381 (1978).
[48] M. F. Brown and J. Seelig, Nature **269**, 721 (1977).
[49] H. Akutsu and J. Seelig, Biochemistry **20**, 7366 (1981).
[50] C. Altenbach and J. Seelig, Biochemistry **23**, 3913 (1984).
[51] M. Roux and M. Bloom, Biochemistry **29**(30), 7077 (1990).
[52] M. Roux and M. Bloom, Biophysical Journal **60**(1), 38 (1991).
[53] H. U. Gally, W. Niederberger, and J. Seelig, Biochemistry **14**(16), 3647 (1975).
[54] P. G. Scherer and J. Seelig, Biochemistry **28**, 7720 (1989).
[55] J. L. Browning and H. Akutsu, Biochimica et Biophysica Acta (BBA) - Biomembranes **684**(2), 172 (1982).
[56] E. C. Kelusky and I. C. Smith, Mol. Pharmacol. **26**(2), 314 (1984).
[57] M. Roux, J. M. Neumann, R. S. Hodges, P. F. Devaux, and M. Bloom, Biochemistry **28**(5), 2313 (1989).
[58] E. Kuchinka and J. Seelig, Biochemistry **28**(10), 4216 (1989).
[59] (2014), manuscript in preparation based on results in nmrlipids.blogspot.fi.
[60] T. Gowers and M. Nielsen, Nature **461**, 879 (2009).
[61] O. H. Samuli Ollila, ArXiv e-prints (2013), 1309.2131.
[62] J. Seelig, Quarterly Reviews of Biophysics **10**, 353 (1977).
[63] M. Hong, K. Schmidt-Rohr, and A. Pines, Journal of the American Chemical Society **117**(11), 3310 (1995).
[64] J. D. Gross, D. E. Warschawski, and R. G. Griffin, Journal of the American Chemical Society **119**(4), 796 (1997).
[65] S. V. Dvinskikh, V. Castro, and D. Sandstrom, Phys. Chem. Chem. Phys. **7**, 607 (2005).
[66] A. Vogel and S. Feller, The Journal of Membrane Biology **245**(1), 23 (2012), ISSN 0022-2631.
[67] S. Ollila, M. T. Hyvönen, and I. Vattulainen, J. Phys. Chem. B **111**, 3139 (2007).
[68] T. M. Ferreira, O. H. S. Ollila, R. Pigliapochi, A. Dabkowska, and D. Topgaard, *Model-free estimation of the effective correlation time for CH bondreorientation in amphiphilic bilayers: 1H13C solid-state NMR and MD simulations*, Accepted to be published in The Journal of Chemical Physics (2015).
[69] B. Hess, C. Kutzner, D. van der Spoel, and E. Lindahl, J. Chem. Theory Comput. **4**, 435 (2008).
[70] S. Plimpton, Journal of Computational Physics **117**(1), 1 (1995).
[71] O. H. S. Ollila (2014), URL `http://dx.doi.org/10.5281/zenodo.13279`.
[72] S.-J. Marrink, O. Berger, P. Tieleman, and F. Jähnig, Biophysical Journal **74**(2), 931 (1998).
[73] J. Määttä (2015), URL `http://dx.doi.org/10.5281/zenodo.13934`.
[74] A. A. Gurtovenko, M. Patra, M. Karttunen, and I. Vattulainen, Biophysical Journal **86**(6), 3461 (2004).
[75] M. S. Miettinen (2013), URL `http://dx.doi.org/10.6084/m9.figshare.829642`.
[76] M. S. Miettinen, A. A. Gurtovenko, I. Vattulainen, and M. Karttunen, The Journal of Physical Chemistry B **113**(27), 9226 (2009).
[77] O. O. H. Samuli and M. Miettinen (2015), URL `http://dx.doi.org/10.5281/zenodo.13944`.
[78] M. Javanainen (2014), URL `http://dx.doi.org/10.5281/zenodo.13497`.
[79] O. H. S. Ollila and M. Retegan (2015), URL `http://dx.doi.org/10.5281/zenodo.13791`.
[80] C. J. Dickson, B. D. Madej, . A. Skjevik, R. M. Betz, K. Teigen, I. R. Gould, and R. C. Walker, Journal of Chemical Theory and Computation **10**(2), 865 (2014).
[81] O. H. S. Ollila and M. Retegan, *MD simulation trajectory and related files for POPC bilayer (Lipid14, Gromacs 4.5)* (2014), URL `http://dx.doi.org/10.5281/zenodo.12767`.
[82] D. Poger, W. F. Van Gunsteren, and A. E. Mark, Journal of Computational Chemistry **31**(6), 1117 (2010).
[83] P. Fuchs, *Temporary location for simulations files with Poger et al. model.* (2014), URL `http://www.dsimb.inserm.fr/~fuchs/project_Samuli/Poger_DPPC/`.
[84] J. P. M. Jämbeck and A. P. Lyubartsev, The Journal of Physical Chemistry B **116**(10), 3164 (2012).
[85] J. Määttä (2014), URL `http://dx.doi.org/10.5281/zenodo.13287`.
[86] A. Kukol, Journal of Chemical Theory and Computation **5**(3), 615 (2009).
[87] M. Javanainen (2014), URL `http://dx.doi.org/10.5281/zenodo.13393`.
[88] S.-W. Chiu, S. A. Pandit, H. L. Scott, and E. Jakobsson, The Journal of Physical Chemistry B **113**(9), 2748 (2009).
[89] A. L. Rabinovich and A. P. Lyubartsev, Journal of Physics: Conference Series **510**(1), 012022 (2014).
[90] J. P. Ulmschneider and M. B. Ulmschneider, Journal of Chemical Theory and Computation **5**(7), 1803 (2009).
[91] M. Javanainen (2014), URL `http://dx.doi.org/10.5281/zenodo.13392`.
[92] R. Tjörnhammar and O. Edholm, Journal of Chemical Theory and Computation **0**(0), null (2014).
[93] M. Javanainen, *DPPC @ 323K, new FF by Tjörnhammar and Edholm* (2014), URL `http://dx.doi.org/10.5281/zenodo.12743`.
[94] J. Henin, W. Shinoda, and M. L. Klein, The Journal of Physical Chemistry B **112**(23), 7008 (2008).
[95] S. Lee, A. Tran, M. Allsopp, J. B. Lim, J. Henin, and J. B. Klauda, The Journal of Physical Chemistry B **118**(2), 547 (2014).
[96] A. Botan (2015), URL `http://dx.doi.org/10.5281/zenodo.13821`.
[97] O. H. S. Ollila (2015), URL `http://dx.doi.org/10.5281/zenodo.13814`.
[98] O. O. H. Samuli and M. Miettinen (2015), URL `http://dx.doi.org/10.5281/zenodo.13946`.
[99] O. O. H. Samuli and M. Miettinen (2015), URL `http://dx.doi.org/10.5281/zenodo.13945`.
[100] M. Javanainen (2014), URL `http://dx.doi.org/10.5281/zenodo.13498`.
[101] O. H. S. Ollila (2015), URL `http://dx.doi.org/10.5281/zenodo.13853`.
[102] M. Höltje, T. Förster, B. Brandt, T. Engels, W. von Rybinski, and H.-D. Höltje, Biochim. Biophys. Acta - Biomembranes **1511**, 156 (2001).

[103] O. H. S. Ollila (2014), URL http://dx.doi.org/10.5281/zenodo.13282.
[104] O. H. S. Ollila (2014), URL http://dx.doi.org/10.5281/zenodo.13281.
[105] O. H. S. Ollila (2014), URL http://dx.doi.org/10.5281/zenodo.13283.
[106] O. H. S. Ollila (2014), URL http://dx.doi.org/10.5281/zenodo.13285.
[107] O. H. S. Ollila (2014), URL http://dx.doi.org/10.5281/zenodo.13286.
[108] J. B. Lim, B. Rogaski, and J. B. Klauda, The Journal of Physical Chemistry B **116**(1), 203 (2012).
[109] M. Javanainen (2015), URL http://dx.doi.org/10.5281/zenodo.13877.
[110] D. Warschawski and P. Devaux, European Biophysics Journal **34**(8), 987 (2005), ISSN 0175-7571.
[111] A. K. Engel and D. Cowburn, FEBS Letters **126**, 169 (1981).
[112] R. J. Mashl, H. L. Scott, S. Subramaniam, and E. Jakobsson, Biophysical Journal **81**(6), 3005 (2001).
[113] A. Pertsin, D. Platonov, and M. Grunze, J. Chem. Phys. **122**, 244708 (2005).
[114] A. Pertsin, D. Platonov, and M. Grunze, Langmuir **23**, 1388 (2007).
[115] C. Eun and M. L. Berkowitz, J. Phys. Chem. B **113**, 13222 (2009).
[116] C. Eun and M. L. Berkowitz, J. Phys. Chem. B **114**, 3013 (2010).
[117] E. Schneck, F. Sedlmeier, and R. R. Netz, Proc. Natl. Acad. Sci. USA **109**, 14405 (2012).
[118] J. N. Israelachvili, *Intermolecular and Surface Forces* (Academic Press, London, 1985).
[119] J. N. Israelachvili and H. Wennerström, Nature **379**, 219 (1996).
[120] E. Sparr and H. Wennerström, Curr. Opin. Colloid Interf. Science **16**(6), 561 (2011).
[121] J. Huang and G. W. Feigenson, Biophys. J. **76**, 2142 (1999).
[122] Q. Zhu, K. H. Cheng, and M. W. Vaughn, The Journal of Physical Chemistry B **111**(37), 11021 (2007).
[123] T. Rog, M. Pasenkiewicz-Gierula, I. Vattulainen, and M. Karttunen, Biochim. Biophys. Acta - Biomembranes **1788**, 97 (2009).
[124] M. Alwarawrah, J. Dai, and J. Huang, J. Chem. Theor. Comput. **8**, 749 (2012).
[125] Biochimica et Biophysica Acta (BBA) - Biomembranes **1798**(3), 688 (2010).
[126] K. Simons and W. L. Vaz, Ann. Rev. Biophys. Biomol. Struct. **33**, 269 (2004).
[127] P. Somerharju, J. A. Virtanen, K. H. Cheng, and M. Hermansson, Biochim. Biophys. Acta - Biomembranes **1788**, 12 (2009).
[128] Biochimica et Biophysica Acta (BBA) - Biomembranes **691**(1), 151 (1982).
[129] T. M. Ferreira, D. Topgaard, and O. H. S. Ollila, Langmuir **30**(2), 461 (2014).
[130] D. P. Tieleman, H. J. Berendsen, and M. S. Sansom, Biophysical Journal **76**(4), 1757 (1999).
[131] M. Bachar, P. Brunelle, D. P. Tieleman, and A. Rauk, J. Phys. Chem. B **108**, 7170 (2004).
[132] D. P. Tieleman, J. L. MacCallum, W. L. Ash, C. Kandt, Z. Xu, and L. Monticelli, J. Phys. Condens. Matter **18**, S1221 (2006).
[133] B. Hess, H. Bekker, H. J. C. Berendsen, and J. G. E. M. Fraaije, J. Comput. Chem. **18**, 1463 (1997).
[134] B. Hess, Journal of Chemical Theory and Computation **4**(1), 116 (2008).
[135] T. Darden, D. York, and L. Pedersen, The Journal of Chemical Physics **98**(12) (1993).
[136] U. L. Essman, M. L. Perera, M. L. Berkowitz, T. Larden, H. Lee, and L. G. Pedersen, J. Chem. Phys. **103**, 8577 (1995).
[137] G. Bussi, D. Donadio, and M. Parrinello, The Journal of Chemical Physics **126**(1) (2007).
[138] H. J. C. Berendsen, J. P. M. Postma, W. F. van Gunsteren, A. DiNola, and J. R. Haak, J. Chem. Phys. **81**, 3684 (1984).
[139] J. P. M. Jämbeck and A. P. Lyubartsev, Journal of Chemical Theory and Computation **8**(8), 2938 (2012).
[140] S. Jo, T. Kim, V. G. Iyer, and W. Im, Journal of Computational Chemistry **29**(11), 1859 (2008).
[141] W. L. Jorgensen, J. Chandrasekhar, J. D. Madura, R. W. Impey, and M. L. Klein, The Journal of Chemical Physics **79**(2) (1983).
[142] M. Parrinello and A. Rahman, J. Appl. Phys. **52**, 7182 (1981).
[143] S. Nose, Mol. Phys. **52**, 255 (1984).
[144] W. G. Hoover, Phys. Rev. A **31**, 1695 (1985).
[145] J. Domaski, P. Stansfeld, M. Sansom, and O. Beckstein, The Journal of Membrane Biology **236**(3), 255 (2010), ISSN 0022-2631.
[146] A. Sousa da Silva and W. Vranken, BMC Research Notes **5**(1), 367 (2012).
[147] R. Salomon-Ferrer, D. A. Case, and R. C. Walker, Wiley Interdisciplinary Reviews: Computational Molecular Science **3**(2), 198 (2013).
[148] H. J. C. Berendsen, J. P. M. Postma, W. F. van Gunsteren, and J. Hermans, *Intermolecular Forces* (Reidel, Dordrecht, 1981), chap.Interaction models for water in relation to protein hydration, pp. 331–342.
[149] I. G. Tironi, R. Sperb, P. E. Smith, and W. F. van Gunsteren, The Journal of Chemical Physics **102**(13) (1995).
[150] P. Fuchs, *Poger lipids with Reaction Field using different GROMACS versions* (2014), URL http://www.dsimb.inserm.fr/~fuchs/project_Samuli/Poger_DPPC/tests_gmx_versions/Comments_area_differ
[151] S. Miyamoto and P. A. Kollman, J. Comput. Chem **13**, 952 (1992).
[152] J. P. M. Jambeck and A. P. Lyubartsev, Phys. Chem. Chem. Phys. **15**, 4677 (2013).

## SUPPLEMENTARY INFORMATION

### 1. Simulation details

#### *a. Berger based models*

For the berger based models we use here the following naming convention: Berger - {*molecule name*} - {*year when model published first time*} {*citation*}. The reason is that there are several different molecular topologies which are using the non-bonded parameters originally developed by Berger et al. [43]. Thus the common factor in the berger based models are the non-bonded parameters, while the molecule specific parameters might somewhat vary. However, the majority of the molecular level topologies are relying (especially for the glycerol backbone and headgroup) on the parameters originally introduced by Marrink et al. [72]. This is the case for all the Berger based simulations discussed in this work.

POPC simulations at full hydration in 298 K and simulations as a function of cholesterol are the same as previous publications [35, 68]. In these simulation the POPC parameters introduced by Ollila et al [67] are used, which are using Berger non-bonded parameters [43] and molecular topology is from Tieleman et al. [130] with improved double bond dihedrals by Bachar et al. [131]. Thus they are called Berger-POPC-07 [67]. The cholesterol model is based on the parameters by Höltje et al. [102] with the exeption that the atom types were changed from CH2/CH3 to LP2/LP3 to avoid overcondensation of the bilayer as suggested in ref. [132]. Since this modification was introduced by Ferreira et al. [35], we call the used cholesterol model as Höltje-CHOL-13 [35].

For the POPC at 323 K and POPC in low hydration the same force field parameters are used. For DPPC the implementation of Berger parameters [43] by Peter Tieleman et al. are used [72]. For all of these simulations the timestep of 2 fs was used with leap-frog integrator. Covalent bond lengths were constrained with LINCS algorithm [133, 134]. Coordinates were written every 10 ps. PME [135, 136] with real space cut-off at 1.0 nm was used for electrostatics. Plain cut-off was used for the Lennard-Jones interactions with a 1.0 nm cut-off. The neighbour lists were updated every 5th step with cut-off at 1.0 nm. Temperature was coupled separately for lipids and water to 298 K with the velocity-rescale method [137] with coupling constant 0.1 ps. Pressure was semi-isotropically coupled to the atmospheric pressure with the Berendsen method [138].

#### *b. CHARMM36*

*DPPC*

Timestep of 1 fs was used with leap-frog integrator. Covalent bonds with hydrogens were constrained with LINCS algorithm [133, 134]. Coordinates were written every 5 ps. PME [135, 136] with real space cut-off at 1.4 nm was used for electrostatics. Lennard-Jones interactions were switched to zero between 0.8 nm and 1.2 nm. The neighbour lists were updated every 5th step with cut-off 1.4 nm. Temperature was coupled separately for lipids and water to 303 K with the velocity-rescale method [137] with coupling constant 0.2 ps. Pressure was semi-isotropically coupled to the atmospheric pressure with the Berendsen method [138].

*POPC* The starting structures for the pure POPC and DOPC simulations was taken from the Slipids [139] website (http://people.su.se/∼jjm/Stockholm_Lipids/Downloads.html). The starting structures for mixed POPC/Cholesterol simulations were constructed with the ChARMM-GUI website [140]. They contained 100 POPC/24 Cholesterol molecules and 80 POPC/80 Cholesterol molecules for the simulations of 20% Cholesterol and 50% Cholesterol respectively. The TIP3P water model [141] was used to solvate the system. The publicly available CHARMM36 forcefield parameters (http://www.gromacs.org/@api/deki/files/184/=charmm36.ff_4.5.4_ref.tgz) by Piggot et al. [6] were used. Cholesterol parameters came from Lim et al. [108] and were converted into Gromacs files by using the PyTopol tool (https://github.com/resal81/PyTopol). Single point energy calculation was done to assess the conversion. Simulations were performed for 200ns and the last 100ns was used for the calculations. Timestep of 2fs was used with leap-frog integrator. All bond lengths were constrained with LINCS [133, 134]. Temperature was maintened at 303 K with the velocity-rescale method [137] and a time constant of 0.2 ps. Pressure was maintained semiisotropically at 1 bar using the Parrinello-Rahman algorithm [142] with a time constant of 1.0 ps. The neighbour list was updated every 10th step with a cut-off of 1.2 nm. Lennard-Jones interactions were switched to zero between 0.8 nm and 1.2 nm. PME [135, 136] with real space cut-off at 1.2nm was used for electrostatics.

#### *c. MacRog*

The lipid force field parameters were obtained from the developers and they correspond to the published DPPC parameters [37] with the inclusion of the double bond parameters. This inclusion of unsaturated lipid tails will be published in the near future.

A bilayer with 288 POPC lipids was hydrated with 12600 TIP3P water [141] molecules (∼44/lipid) and simulated for 100 ns with a time step of 2 fs. Data was saved every 10 ps and the first 20 ns of the trajectory was discarded from the analysis. All bond lengths were constrained with LINCS [133, 134]. The temperatures of the lipids and the solvent were separately coupled to the Nosé–Hoover thermostat [143, 144] with a target temperature of 310 K and a time constant of 0.4 ps. Semi-isotropical pressure coupling to 1 bar was obtained with the Parrinello–Rahman barostat [142] with a time constant of 1 ps. PME [135, 136] was employed to calculate the long-range electrostatic interactions. Lennard-Jones interactions were cut off at 1 nm and the dispersion correction was applied to both energy and pressure. A neighbour list with a radius of 1 nm was updated every step.

Identical parameters were employed for both full hydration and for the dehydration simulations. The dehydration simulations were also run for 100 ns with data saved every 10 ps.

The initial structures for the simulations with 10, 40, 50 and 60 mol% of cholesterol were obtained by replacing 14, 56, 64 or 72 POPC molecules with cholesterol molecules in the initial structure containing 128 POPC molecules. These systems were simulated for 400 ns and the first 200 ns was discarded from analysis. Data was saved every 100 ps.

#### *d. GAFFLipid*

The initial structure in Lipidbook [145] had different glycerol backbone isomers in different leaflets. To generate the initial structure we took the structure delivered by Slipid developers [139]. Also this structure had one lipid with different glycerol bakcbone isomer. This lipid and one lipid from opposite leaflet were removed after the system was equilibrated.

The force field parameters were generated using files obtained from the Lipidbook website (http://lipidbook.bioch.ox.ac.uk/package/show/id/150.html) [145]. The conversion to Gromacs compatible formats was performed using the acpype tool [146]. The accuracy of the conversion was checked by calculating the total energy of a single POPC lipid molecule using the sander program which is part of the AmberTools14 package [147] and Gromacs 4.6.5. A difference of 0.002 kcal/mol was obtained between the two programs.

Timestep of 2 fs was used in Langevin dynamics with zero friction term and collision frequency of 1.0 $ps^{-1}$. Covalent bonds with hydrogens were constrained with LINCS algorithm [133, 134]. Coordinates were written every 10 ps. PME [135, 136] with real space cut-off at 1.0 nm was used for electrostatics. Plain cut-off with 1 nm was used for Lennard-Jones interactions. The neighbour lists were updated every 5th step with cut-off 1.0 nm. Pressure was semi-isotropically coupled to the 1 bar pressure with the Berendsen method [138].

#### *e. Lipid14*

The initial structure was taken directly from the Lipidbook [145]. The Amber compatible force field parameters were generated using the tleap program which is integrated in the AmberTools14 package [147]. A workflow similar to the one used previously for the conversion and validation of the GAFFLipid parameters was followed here. As before, a negligible energy difference of 0.003 kcal/mol was obtained between the two programs.

Timestep of 2 fs was used in Langevin dynamics with zero friction term and collision frequency of 1.0 $ps^{-1}$. Covalent bonds with hydrogens were constrained with LINCS algorithm [133, 134]. Coordinates were written every 10 ps. PME [135, 136] with real space cut-off at 1.0 nm was used for electrostatics. Plain cut-off with 1 nm was used for Lennart-Jones interactions. Dispersion correction was used for energy and pressure. The neighbour lists were updated every 5th step with cut-off 1.0 nm. Pressure was semi-isotropically coupled to the 1 bar pressure with the Berendsen method [138].

#### *f. Poger et al.*

The Poger lipids are derived from GROMOS G53A6 [82] and were initially coined 53A6-L (L for lipids), and are now part of GROMOS G54A7 [34]. They work with the SPC water model [148]. The initial hydrated bilayer structure of 128 DPPC/5841 water molecules as well as force field parameters were downloaded from David Poger's web site (http://compbio.chemistry.uq.edu.au/∼david/) on April 2012. We noticed that the same files downloaded in October 2013 appear to lack two dihedral angles in the choline headgroup (only one dihedral of type gd_29 allowing the rotation of the 3 choline methyls) compared to the April 2012 version (3 dihedrals of type gd_29 for the 3 choline methyls). This should not affect the bilayer structure and only change the kinetics of the choline methyls rotation, however the October 2013 version has not been tested.

MD Simulations (two repetitions with independent initial velocities) were run for 100 ns using a 2 fs time step and the analysis was performed on the last 50 ns. Coordinates were saved every 50 ps for analysis. All bond lengths were constrained with the LINCS algorithm [133, 134]. Temperature was kept at 323K with the v-rescale [137] thermostat with a time constant of 0.1 ps (DPPC and water coupled separetly). Pressure was maintained semi-isotropically at 1 bar using the Parrinello-Rahman

barostat [142] using a 4 ps time constant and a compressibility of 4.5e-5 $bar^{-1}$. For non-bonded interactions, two conditions were tested: i) A 0.8-1.4 nm twin-range cutoff with the neighbor list updated every 5 steps for both electrostatics and Lennard-Jones. For the former the generalized reaction field (RF) with a dielectric permitivity of 62 was used beyond the 1.4 nm cutoff [149]. This is the original setup that Poger et al. [82] used. ii) PME [135, 136] electrostatics with a real space cutoff of 1.0 nm, a Fourier spacing of 0.12 nm and an interpolation order of 4, LJ computed with a 1.0-1.4 nm twin-range cutoff, neighbor list updated every 5 steps. Note that Poger and Mark tested the effect of PME vs RF in the ref. [34], but used a 1.0 nm cutoff with PME and 1.4 nm with RF for LJ interactions. Since 0.8-1.4 nm twin-range cutoff for LJ interations is used in the parametrization of GROMOS force field we decided to use that also in the simulations with PME.

Since Poger lipids come from GROMOS force field, it is important to note that GROMOS uses the RF scheme for computing electrostatics (this is the method used for the force field parameterization). Using setup i) based on RF, we were able to reproduce the results (i.e. area per lipid 0.63 $nm^2$) from the original work only with GROMACS version $<= 4.0.*$ (the original authors [82] used GROMACS version 3.3.3). On going to versions $>= 4.5.*$, the area per lipid dropped below 0.58 $nm^2$. The GROMACS developers were contacted and a redmine issue opened (http://redmine.gromacs.org/issues/1400). The difference comes from the new Trotter decomposition introduced in version 4.5. A fix has been introduced in version 4.6.6 that allows a recovery of 0.615 $nm^2$. The results in terms of area per lipid using the different GROMACS versions are here [150]. Thus we decided to use only the PME setup ii) for computing the order parameter since it gives stable results whatever the GROMACS version. We obtained an area per lipid of 0.615 $nm^2$, below 0.648 $nm^2$ found by the original authors with their PME setup (see [34]). We explained that by the fact we used a 1.4 nm for the LJ cutoff and they used 1.0 nm.

### *g. Slipid*

Initial coordinates for a hydrated DPPC bilayer (30 waters/lipid) at 323K were taken directly from http://people.su.se/$\tilde{}$jjm/Stockholm_Lipids/Downloads.html The Slipids force field [84] was used for the the all atom description of DPPC, and water was described with the TIP3P water model [141]. Simulations were performed within the NPT ensemble using the GROMACS 4.6.1 simulation package [69]. The nose–hoover rescaling thermostat [143, 144] was used with reference temperature of 323 K and a relaxation time constant of 0.5 ps. Water and lipids were coupled separately to the heat bath. Pressure was kept constant at 1.013 bar using a semi–isotropic Parinello–Rahman barostat [142] with a time constant of 10.0 ps. Equations of motion were integrated with the leapfrog algorithm using a timestep of 2 fs. Long range electrostatic interactions were calculated using the PME method [135, 136], with a fourth order smoothing spline. A real space cutoff of 1.0 nm was employed with grid spacing of 0.12 in the reciprocal space. Lennard–Jones potentials were cutoff at 1.4 nm, with dispersion correction applied both to energy and pressure. All covalent bonds in lipids were constrained using the LINCS algorithm [133], whereas water molecules were constrained using SETTLE [151]. Twinrange cutoffs, 1.0 nm and 1.6 nm, were used for the neighborlists with the longrange neighbor list updated every 10 steps. This simulation protocol corresponds to the protocol used in Ref [152].

### *h. Kukol*

A bilayer patch with 512 POPC lipids was constructed and hydrated with $\sim$40 SPC water molecules per lipid. The force field parameters were obtained from Lipidbook [145]. This bilayer was simulated with a 2 fs time step for a total of 50 ns and coordinates were saved every 100 ps. All bonds were constrained with LINCS [133, 134]. PME [135, 136] was employed for the long-range electrostatics. Lennard-Jones interactions were cut off at 1.4 nm. A neighbour list with a radius of 0.8 nm was updated every 5 steps. The constant temperature of 298 K was maintained with the Berendsen thermostat [138] with a time constant of 0.1 ps. The Berendsen barostat [138] was employed for semi-isotropical pressure coupling at 1 bar.

### *i. Chiu et al.*

The force field parameters and the initial configuration were available through the Lipidbook [145]. Timestep of 2 fs was used with leap-frog integrator. Covalent bond lengths were constrained with LINCS algorithm [133, 134]. Coordinates were written every 10 ps. PME [135, 136] with real space cut-off at 1.0 nm was used for electrostatics. Twin range cut-off was used for the Lennardt-Jones interactions with short and long cut-offs at 1.0 nm and 1.6 nm, respectively. The neighbour lists were updated every 5th step with cut-off at 1.0 nm. Temperature was coupled separately for lipids and water to 298 K with the velocity-rescale method [137] with coupling constant 0.2 ps. Pressure was semi-isotropically coupled to the atmospheric pressure with the Parrinello-Rahman method [142].

### *j. Ulmschneider*

The initial structure containing 128 POPC molecules with 3328 TIP3P water [141] molecules (26 per lipid) was downloaded from Lipidbook [145] together with the topologies. This bilayer was simulated for 100 ns with a time step of 2 fs and the data was saved every 10 ps. The bonds involving hydrogen atoms were constrained with LINCS [133, 134]. The temperature was kept at 298 K with the Berendsen thermostat [138]. The pressure was semi-isotropically coupled to the Berendsen barostat [138] with a time constant of 1 ps and a target pressure of 1 bar. PME [135, 136] was employed for long range electrostatics and a cut-off of 1 ns was employed for the Lennard-Jones interactions. A neighbour list with a radius of 1 nm was updated every 10 steps.

Additionally, the simulations were repeated with the dispersion correction applied to pressure and temperature. Even though the area per lipid decrease d slightly, the head group order parameters were only slightly affected.

### *k. Tjörnhammar et al.*

The gel phase structure delivered by Tjörnhammar and edholm [92] was ran a 5ns at 70 degrees in order to destroy the ordered gel configuration. This was followed by 200ns simulation at 50 degrees. The last 100ns of this simulation was used for analysis. The same mdp file as in the paper's [92] SI was used except for the temperatures.

### *l. CHARMM36-UA*

A hydrated bilayer consisting of 128 DLPC lipids and 3840 water molecules is modeled by the force field of Lee and co-workers [95], which is a combination of the all-atom CHARMM36 force-field [31] and the united-atom Berger model [43]. The nonbonding interactions are calculated using an atom-based switching function with inner and outer cutoffs of 0.8 and 1.2 nm [95]. Long range electrostatic interactions are implemented using the particle-particle particle-mesh solver with a relative accuracy of 0.0001. The system is first equilibrated for 30 ns in the NP$\gamma$T ensemble (Nose-Hoover [143, 144] style thermostat and barostat with anisotropic pressure coupling) at 323 K and 1 bar with timestep of 1 fs, the next 20 ns of dynamics are taken for calculation of configurational averages. Simulations were carried out by using the LAMMPS package [70].

## 2. Dihedral angle distributions as a function of cholesterol in CHARMM36

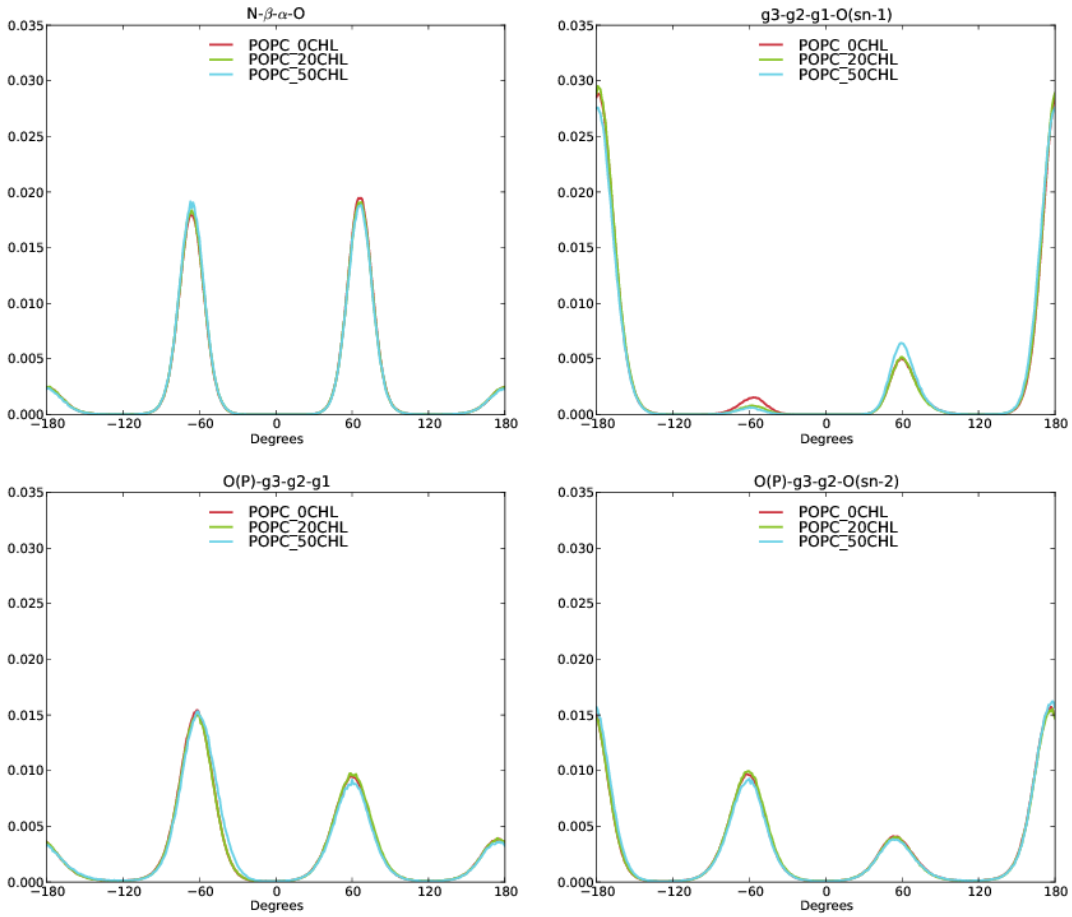



FIG. 9. The effect of cholesterol content on the glycerol backbone and choline dihedral angles in CHARMM36 model.